ACS Partner Journal

CHEM & BIO ENGINEERING



pubs.acs.org/ChemBioEng

Article

# Destructive Adsorption of Nitrogen Trifluoride ($NF_3$) Using M-MOF-74 with Open Metal Sites

*Published as part of Chem & Bio Engineering virtual special issue "Advanced Separation Materials and Processes".*

Shao-Min Wang,[§] Qian Zhang,[§] Yi-Tao Li, Si-Chao Liu, and Qing-Yuan Yang*

Cite This: *Chem Bio Eng.* 2024, 1, 535−540

Read Online

ACCESS | Metrics & More | Article Recommendations | Supporting Information

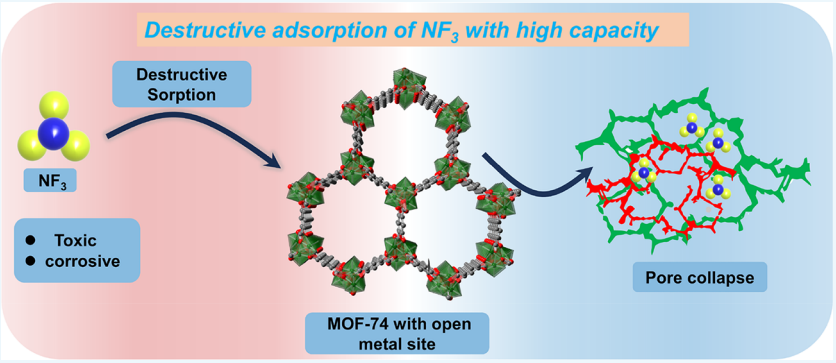


**ABSTRACT:** Using solid adsorbents for the destructive sorption of nitrogen trifluoride ($NF_3$) presents a potential solution to its dual challenges as a potent greenhouse gas and hazardous compound in microelectronics. In this study, a series of MOFs (M-MOF-74, M = Mg, Co, Ni, Zn) with open metal sites (OMSs) are utilized for $NF_3$ adsorption. By employing single-component adsorption isotherms and the ideal adsorbed solution theory (IAST) selectivity calculations, the adsorption performance of various adsorbents is evaluated. The results indicate that Mg, Co, and Ni-MOF-74 exhibit high adsorption capacities for $NF_3$, while Zn-MOF-74 shows a lower adsorption capacity, likely due to the weaker Lewis acidity of $Zn^{2+}$. Experimental findings from PXRD and gas adsorption studies indicate structural pore alteration in the MOF-74 series following $NF_3$ gas adsorption. Theoretical computational analyses reveal that the MOF-74 series has a higher adsorption affinity for $NF_3$ compared to $N_2$. This research provides insights into the use of efficient MOF sorbents for the destructive adsorption of $NF_3$.

**KEYWORDS:** *metal−organic framework, nitrogen trifluoride, greenhouse gas, open metal sites, adsorption*

## INTRODUCTION

Nitrogen trifluoride ($NF_3$) is a chemically and thermally stable artificial inorganic gas used primarily in the cleaning and etching processes of manufacturing procedures, particularly in the production of large-scale integrated circuits and display panels. However, depending on the specific equipment and application, the utilization efficiency of $NF_3$ in plasma processes varies. A significant amount of reactants is wasted in the exhaust gas stream and subsequently released into the Earth's atmosphere.[1] It is noteworthy that $NF_3$ is a significant greenhouse gas. Although more environmentally friendly than $SF_6$, the global warming potential (GWP) of $NF_3$ is 17,200 times greater than carbon dioxide, with a lifetime in the atmosphere of up to 740 years.[2] Although $NF_3$ has not been included in the Kyoto Protocol, the United Nations Framework Convention on Climate Change has sensibly decided to include $NF_3$ in the second commitment period. Subsequently, the Doha Amendment has included $NF_3$ within the regulated scope, thereby expanding the controlled greenhouse gas portfolio to encompass seven gases. Average atmospheric $NF_3$ concentrations have risen from 0.02 parts per trillion (ppt) in 1978 to 0.454 ppt in 2008, leading to severe greenhouse effects. Also, it is important to note that $NF_3$ is toxic to humans. The Immediately Dangerous to Life or Health (IDLH) value for $NF_3$ is reported to be 1,000 parts per million (ppm).

**Received:** November 24, 2023
**Revised:** February 7, 2024
**Accepted:** February 8, 2024
**Published:** February 16, 2024

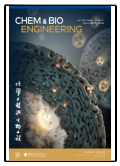

Taking into consideration the greenhouse effect and toxicity of $NF_3$, it should be prioritized to reduce its emissions or facilitate its elimination. The existing methods for treating $NF_3$ waste gases primarily involve high-temperature thermal decomposition or catalytic hydrolysis. However, these methods result in the emission of highly toxic and corrosive gases, which are highly detrimental to the environment and lack environmental friendliness.[3−6] In contrast, destructive sorption of $NF_3$ by using solid adsorbents that could react with $NF_3$ without harmful gas production is a more environmentally friendly approach. The key lies in the development of highly efficient adsorbents.[7−9] Some researchers have employed metal oxides for the destructive adsorption of $NF_3$,[10,11] but the specific surface area of metal oxides is typically not high. Due to the relatively low concentrations of $NF_3$ in waste gas and the atmosphere, adsorbents capable of adsorbing a significant amount of $NF_3$ under low pressure are preferable choices. Metal−organic frameworks (MOFs) have been extensively researched and developed in recent years. Their large specific surface areas and tunable pore sizes make them suitable for gas adsorption and storage applications.[12,13] Most studies in the field of fluorine-containing gas (F-gas) have only focused on the capture of F-gas using MOFs.[14−17] However, considering the toxicity of $NF_3$ gas, implementing permanent destructive adsorption of $NF_3$ would be more effective in reducing its greenhouse effect and mitigating the associated hazards. There are limited examples of utilizing MOFs for permanent destructive adsorption of $NF_3$, primarily due to the lack of reactivity between most MOFs and $NF_3$. MOFs containing open metal sites (OMSs) exhibit Lewis acidic behavior and can participate in chemical reactions with Lewis bases such as $NF_3$. The MOF-74 analogues have demonstrated exceptional properties in the field of gas adsorption and separation, particularly in $CO_2$ adsorption.[18] Bae et al. have previously reported the adsorption characteristics of $SF_6$ on MOF-74 analogues.[19] However, few studies have specifically investigated $NF_3$ sorption on MOF-74.

Here, we utilize a series of MOFs, specifically M-MOF-74, where M is $Mg^{2+}$, $Co^{2+}$, $Ni^{2+}$, and $Zn^{2+}$, containing OMSs to facilitate the destructive adsorption of $NF_3$. Single-component gas adsorption isotherm results showed that Co-MOF-74 demonstrated the highest adsorption capacity. Notably, Co-MOF-7 shows the ultrahigh $NF_3/N_2$ (1/9) separation selectivity of 299.6 (298 K and 100 kPa), which sets a new benchmark for inverse $NF_3/N_2$ separation. The PXRD and $N_2$ sorption results of the post-adsorption MOFs indicate a significant alteration in both the structural framework and pore architecture, implying a chemical interaction between the MOFs and $NF_3$.

## RESULTS AND DISCUSSION

The first MOF-74, also known as Zn-DOBDC, was reported by Yaghi and co-workers.[20] Following the report of Zn/DOBDC, Co/DOBDC,[21] Ni/DOBDC,[22] and Mg/DOBDC[18] were synthesized by other researchers subsequently. These compounds have a crystal structure similar to that of Zn/DOBDC, comprising $M^{II}$ ions that create linear, infinite-rod secondary building units (SBUs) connected by DOBDC ligands, leading to one-dimensional pore structures that are hexagonal in shape (Figure 1a). The synthesized material encompasses pores that are inhabited by solvent molecules, which fulfill the coordination of the $M^{II}$ ions within the matrix. Subsequent evaporated results in the removal of these solvent

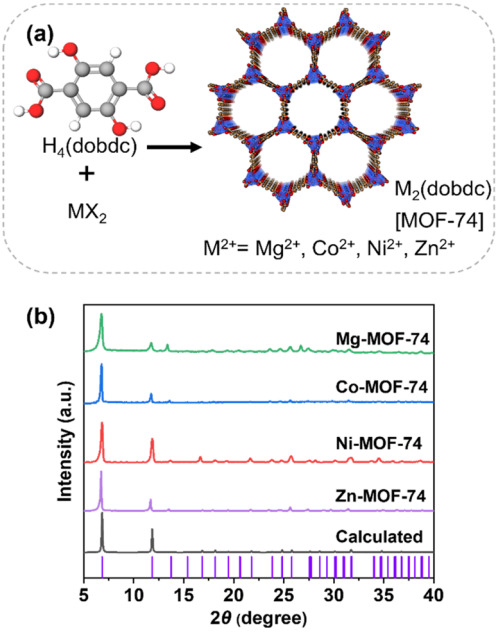


**Figure 1.** (a) The crystal structures and pore structures of MOF-74 with 1D hexagonal channels. (b) PXRD patterns of the as-synthesized M-MOF-74.

molecules, leading to the creation of unsaturated metal sites or OMSs. The phase purity of the synthesized MOF-74 analogues was verified by powder X-ray diffraction (PXRD) analysis, exhibiting a strong agreement with the calculated PXRD pattern, as shown in Figure 1b. The evaluation of the porosities of MOF-74 analogues was performed by sorption of $N_2$ at 77 K. As illustrated in Figure 2, all of the MOFs demonstrate characteristic type-I sorption behaviors, indicating the presence of microporous structures within their frameworks. The saturated $N_2$ adsorption capacities of the four samples are as follows: 360.7 $cm^3\ g^{-1}$ for Mg-MOF-74, 316.2 $cm^3\ g^{-1}$ for Co-MOF-74, 282.8 $cm^3\ g^{-1}$ for Ni-MOF-74, and 260.2 $cm^3\ g^{-1}$ for Zn-MOF-74, respectively. The surface area was determined using the BET (Brunauer−Emmett−Teller) method (Figures S1−S4). Accordingly, the BET surface areas of Mg-MOF-74, Co-MOF-74, Ni-MOF-74, and Zn-MOF-74 were determined to be 784.6, 1313.4, 1080.0, and 941.1 $m^2\ g^{-1}$, respectively. These values exhibit a reasonable agreement with those previously reported in the literature.[23−26] The results suggested the MOF-74 analogues were successfully prepared. In addition, nonlocal density functional theory (NLDFT) modeling reveals that the pore size distribution for Mg-MOF-74 is primarily 9.0 Å, for Co-MOF-74 it is 10.7 Å, for Ni-MOF-74 it is 9.7 Å, and for Zn-MOF-74 it is 10.3 Å (Figure 2), which are in line with the pore aperture of 11 Å obtained from the single-crystal structure.

The single-component gas adsorption isotherms were employed to assess the adsorption capacity of $NF_3$ and $N_2$. As shown in Figure 3a, the amount of $NF_3$ adsorbed quickly increased at low pressure, indicating that Mg-MOF-74 has a stronger $NF_3$ affinity. The Mg-MOF-74 showed an uptake of 50.5 $cm^3\ g^{-1}$ for $NF_3$ and 21.9 $cm^3\ g^{-1}$ for $N_2$ at 298 K and 100 kPa. The adsorption isotherms of $NF_3$ on Co-MOF-74 exhibited a prompt increase in the low-pressure region with an uptake of 54.0 $cm^3\ g^{-1}$ at 10 kPa and 298 K (Figure 3b). The adsorption of $NF_3$ follows the typical type I isotherm, with a total adsorption of 66.6 $cm^3\ g^{-1}$, which is significantly higher


https://doi.org/10.1021/cbe.3c00096
Chem Bio Eng. 2024, 1, 535−540

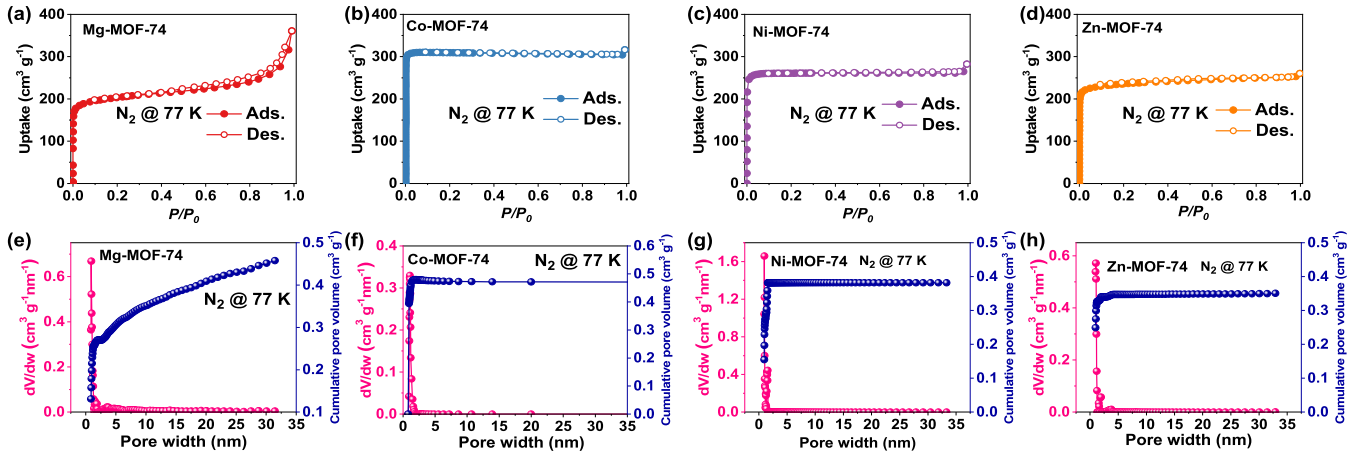


**Figure 2.** $N_2$ sorption isotherms at 77 K on (a) Mg-MOF-74, (b) Co-MOF-74, (c) Ni-MOF-74, and (d) Zn-MOF-74. Pore size distribution and pore volumes curves of (e) Mg-MOF-74, (f) Co-MOF-74, (g) Ni-MOF-74, and (h) Zn-MOF-74.

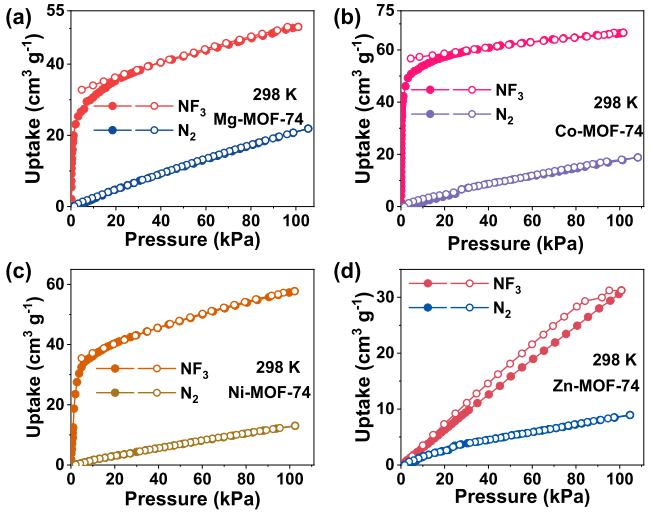


**Figure 3.** Single component $NF_3$ and $N_2$ adsorption isotherms for (a) Mg-MOF-74, (b) Co-MOF-74, (c) Ni-MOF-74, and (d) Zn-MOF-74 at 298 K and 100 kPa.

than that of $N_2$ (18.8 $cm^3\ g^{-1}$). As can be seen from Figure 3c, the uptake of $NF_3$ for Ni-MOF-74 also exhibits a significantly steeper increase under 10 kPa compared to that of $N_2$. At 298 K and 100 kPa, the $NF_3$ and $N_2$ uptakes for Ni-MOF-74 were 57.7 and 13.0 $cm^3\ g^{-1}$, respectively. Unlike the aforementioned three MOFs, Zn-MOF-74 exhibits a linear adsorption isotherm for $NF_3$ (Figure 3d) and the $NF_3$ sorption amount is much smaller. Adsorption isotherms in Figure 3d showed that the amount adsorbed of $NF_3$ and $N_2$ for Zn-MOF-74 were 31 and 8.9 $cm^3\ g^{-1}$, respectively. Despite the four MOF-74 analogues having similar pore sizes, Zn-MOF-74 exhibits significantly different $NF_3$ adsorption behavior. The observed dissimilarity in $NF_3$ adsorption behavior among the four isomers of MOFs with similar pore sizes can potentially be attributed to the diverse extent of interaction between $NF_3$, functioning as a Lewis base, and MOF-74, characterized by distinct Lewis acidities. This difference in Lewis acid−base reactivity may result in contrasting adsorption properties, thereby influencing the overall adsorption isotherms. The $NF_3$ and $N_2$ adsorption isotherms at 273 K and 100 kPa are shown in Figures S5−S8. Both gases' adsorption capacities exhibit an increase under these circumstances. The calculated adsorption heats of $NF_3$ on Mg-MOF-74, Co-MOF-74, Ni-MOF-74, and Zn-MOF-74 at zero loading are 108.8, 61.6, 21.8, and 131.3 kJ/mol (Figure S9), respectively.

To evaluate the gas separation ability of samples, ideal adsorbed solution theory (IAST) calculations of $NF_3/N_2$ (1/9, v/v) mixture adsorption were performed based on the single gas adsorption isotherm. As shown in Figure 4a, the calculated

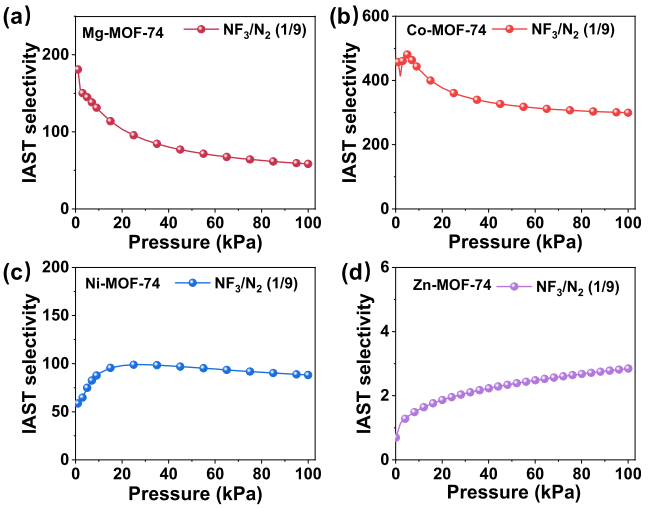


**Figure 4.** IAST-predicted $NF_3/N_2$ (1/9) selectivity on (a) Mg-MOF-74, (b) Co-MOF-74, (c) Ni-MOF-74, and (d) Zn-MOF-74 at 298 K and 0-100 kPa.

IAST selectivity of Mg-MOF-74 under conditions of 298 K and 100 kPa for binary gas mixtures composed of $NF_3/N_2$ (1/9, v/v) was found to be 58.4. In the pressure range 0−100 kPa, the selectivity of Mg-MOF-74 toward $NF_3/N_2$ reduces gradually. This can be attributed to the higher capacity of Mg-MOF-74 for $NF_3$ at lower pressures. As the pressure increases, the capacity for $NF_3$ gradually reaches equilibrium. This reveals the dynamic interaction between pressure and the adsorption behavior of Mg-MOF-74 on $NF_3$. A comparable situation has occurred in both Co-MOF-74 and Ni-MOF-74, in which their selectivities toward $NF_3/N_2$ (1/9, v/v) are 299.6 (Figure 4b) and 88.2 (Figure 4c) at 298 K and 100 kPa, respectively. Owing to Zn-MOF-74's low adsorption capacity and weak adsorption affinity toward $NF_3$, its selectivity for



https://doi.org/10.1021/cbe.3c00096
Chem Bio Eng. 2024, 1, 535−540

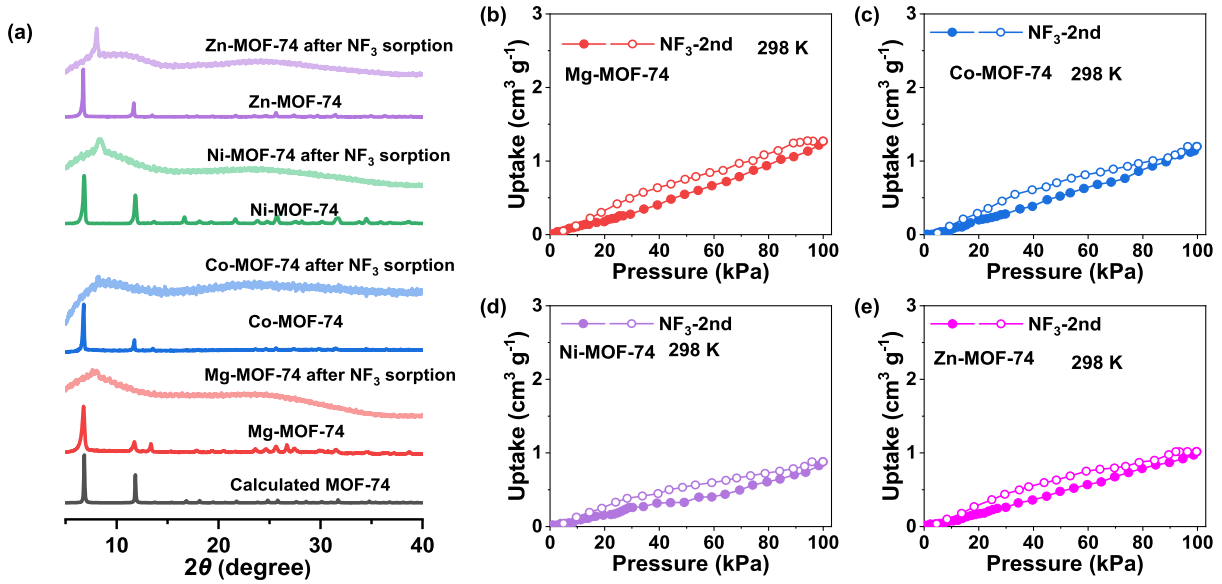


**Figure 5.** (a) The PXRD pattern of M-MOF-74 after $NF_3$ sorption. $NF_3$ adsorption isotherms from the second measurement for (b) Mg-MOF-74, (c) Co-MOF-74, (d) Ni-MOF-74, and (e) Zn-MOF-74 at 298 K.

$NF_3/N_2$ is only 2.8 (Figure 4d) at 298 K and 100 kPa. Co-MOF-74 displays the highest $NF_3/N_2$ selectivity among the four MOFs studied and outperforms several materials previously reported in the literature for $NF_3/N_2$ selectivity, namely, POPTrB-8F (5.7),[27] $Co_3(HCOO)_6$ (19.2),[28] $Mn_3(HCOO)_6$ (20.0),[28] $Ni_3(HCOO)_6$ (30.0),[28] SBMOF-1 (21.0),[29] Ni-MOF (35.8),[14] $NH_2$−Ni-MOF (32.4),[14] PC-750 (61.4),[30] and others. The adsorption curve indicates Co-MOF-74 has a stronger affinity for $NF_3$ at low pressures, with an adsorption capacity of up to 54.0 $cm^3\ g^{-1}$ (2.41 mmol $g^{-1}$) at 10 kPa. This observation suggests significant host−guest interactions.

To verify the occurrence of reverse reaction between $NF_3$ and the MOF-74 series, we conducted tests on the adsorption isotherms of $N_2$ on MOF-74 after $NF_3$ adsorption and the subsequent adsorption isotherm of $NF_3$ for the second time. Additionally, the PXRD patterns of the MOF-74 samples after $NF_3$ adsorption were examined. The crystalline architecture of the MOF-74 series subjected to $NF_3$ adsorption has become compromised, as illustrated by Figure 5a. This outcome elucidates the gas-phase degradation of the crystalline architecture within the MOF-74 series induced by $NF_3$. As shown in Figure 5b−e, the isotherm experiment results for the second instance of single-component $NF_3$ gas adsorption also signify that the MOF-74 series can no longer adsorb $NF_3$ gas. Conducting nitrogen adsorption tests at a low temperature of 77 K on the MOF-74 series that has undergone $NF_3$ adsorption revealed that all the MOF-74 series no longer exhibit a microporous structure (Figures S10−S13). This observation underscores the disruptive adsorptive capability of MOF-74 toward $NF_3$ gas, thereby potentially mitigating the atmospheric impact of $NF_3$ emissions.

The SEM images of Ni-MOF-74 and Zn-MOF-74 sorbents as examples are shown in Figure 6. Before the adsorption of $NF_3$ gas, the surfaces of these two MOFs exhibited a sleek and well-defined morphology (Figure 6a,c). Following the adsorption of $NF_3$ gas, the surfaces of these two MOFs transformed, exhibiting a notably roughened texture (Figure 6b,d). From the analysis using energy dispersive X-ray

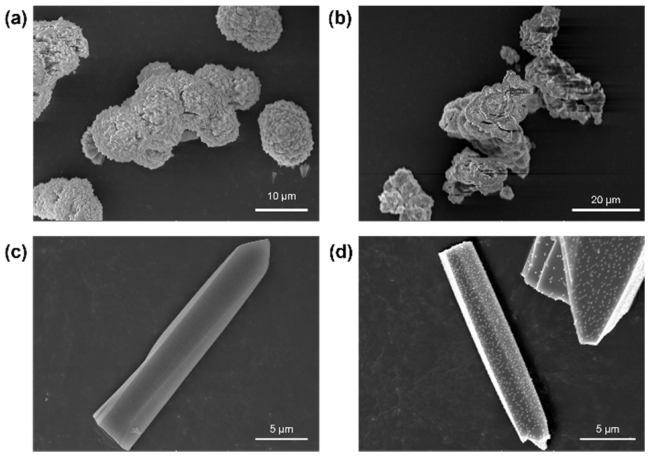


**Figure 6.** SEM images of (a) Ni-MOF-74, (b) spent Ni-MOF-74, (c) Zn-MOF-74, and (d) spent Zn-MOF-74.

spectroscopy (EDS) (Figures S14−S21), it is evident that the concentration of F significantly increases within the spent MOF samples after $NF_3$ adsorption.

Figure 7 illustrates the proposed $NF_3$ destructive sorption mechanism on M-MOF-74. Based on the preceding experimental outcomes, it is discernible that following the

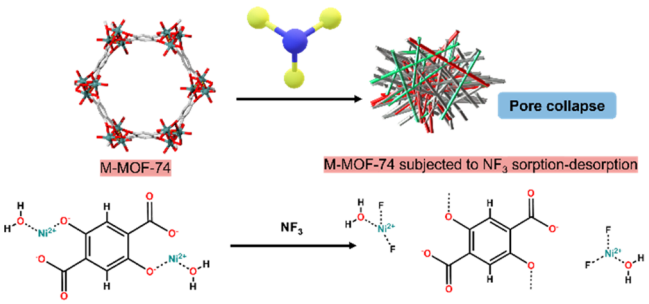


**Figure 7.** Schematic illustration of the proposed $NF_3$ destructive sorption mechanism on M-MOF-74.


https://doi.org/10.1021/cbe.3c00096
Chem Bio Eng. 2024, 1, 535−540

adsorption−desorption of $NF_3$ gas, the framework of M-MOF-74 experiences structural collapse. This potential explanation derives from the interaction between $NF_3$ gas molecules and MOF-74 metal sites.

In order to gain a better insight into the adsorption interactions between the gases and their adsorption sites, grand Canonical Monte Carlo (GCMC) simulations were performed. As shown in Figure 8, the intermolecular distances between

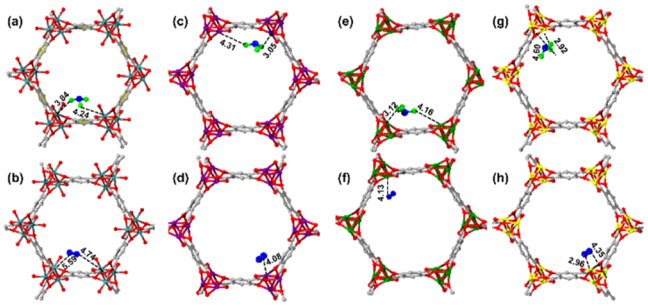


**Figure 8.** Calculated binding sites for (a) $NF_3$, (b) $N_2$ on Mg-MOF-74, (c) $NF_3$, (d) $N_2$ on Co-MOF-74, (e) $NF_3$, (f) $N_2$ on Ni-MOF-74, (g) $NF_3$, and (h) $N_2$ on Zn-MOF-74.

$NF_3$ molecules and the MOF-74 series are uniformly shorter than those between $N_2$ molecules and MOF-74. The observation suggests that MOF-74 has a higher affinity for $NF_3$ molecules.

## CONCLUSIONS

$NF_3$ is of great industrial significance; however, its emissions have severe implications for greenhouse gas emissions and public health. Mitigating the risks associated with $NF_3$ necessitates adopting an effective strategy such as destructive adsorption using solid adsorbents. In this investigation, we utilized the MOF-74 materials, featuring accessible metal sites, for $NF_3$ adsorption. Our experimental findings revealed that Mg, Co, and Ni-MOF-74 exhibit remarkable adsorption capacities for $NF_3$, while Zn-MOF-74 displayed comparatively lower adsorption efficiency. Co-MOF-74 was found to adsorb up to 54.0 $cm^3\ g^{-1}$ of $NF_3$ at 10 kPa and 298 K. Simultaneously, it demonstrated the highest selectivity, reaching up to 299.6. This discrepancy can be attributed to variations in the acidity of the different metals, influencing their affinity for $NF_3$. This study sheds light on the potential of destructive adsorption for addressing $NF_3$ emissions, thereby contributing to innovative approaches for tackling this issue.

## ASSOCIATED CONTENT

### Supporting Information

The Supporting Information is available free of charge at https://pubs.acs.org/doi/10.1021/cbe.3c00096.

Synthetic details, characterization details, computational details, figures of BET fitting, adsorption−desorption isotherms, $Q_{st}$ curves, EDS analysis, and elemental mappings, Langmuir−Freundlich fitting, tables of element content, and comparison of adsorption characteristics (PDF)

## AUTHOR INFORMATION


### Corresponding Author

**Qing-Yuan Yang** − *School of Chemical Engineering and Technology, Xi'an Jiaotong University, Xi'an 710049, China;* orcid.org/0000-0002-1742-2088; Email: qingyuan.yang@xjtu.edu.cn

### Authors

**Shao-Min Wang** − *School of Chemical Engineering and Technology, Xi'an Jiaotong University, Xi'an 710049, China*

**Qian Zhang** − *High & New Technology Research Center of Henan Academy of Sciences, Zhengzhou 450052 Henan Province, China*

**Yi-Tao Li** − *School of Chemical Engineering and Technology, Xi'an Jiaotong University, Xi'an 710049, China*

**Si-Chao Liu** − *School of Chemical Engineering and Technology, Xi'an Jiaotong University, Xi'an 710049, China*

Complete contact information is available at: https://pubs.acs.org/10.1021/cbe.3c00096

### Author Contributions

§S.M.W. and Q.Z. contributed equally to this work.


### Notes

The authors declare no competing financial interest.

## ACKNOWLEDGMENTS

This work was financially supported by the National Natural Science Foundation of China (No. 22371221). Qing-Yuan Yang acknowledges the China National Key R&D Program (2022YFB4003701), China Tobacco Anhui Industrial Co., Ltd. (2022162), and Shccig-Qinling Program (SMYJY20220582).

## REFERENCES


(1) Donnelly, V. M.; Flamm, D. L.; Dautremont-Smith, W.; Werder, D. Anisotropic etching of $SiO_2$ in low-frequency $CF_4/O_2$ and $NF_3$/Ar plasmas. *J. Appl. Phys.* **1984**, *55*, 242−252.

(2) Prather, M. J.; Hsu, J. $NF_3$, the greenhouse gas missing from Kyoto. *Geophys. Res. Lett.* **2008**, *35*, No. L12810.

(3) Kim, J. H.; Cho, C. H. Study on the Oxidant effect for nitrogen trifluoride abatement by using a 2.45 GHz microwave plasma torch. *J. Korean Phys. Soc.* **2020**, *76*, 895−898.

(4) Jeon, J. Y.; Xu, X.-F.; Choi, M. H.; Kim, H. Y.; Park, Y.-K. Hydrolytic decomposition of PFCs over $AlPO_4$−$Al_2O_3$ catalyst. *Chem. Commun.* **2003**, 1244−1245.

(5) Wang, J.; Fu, W.; Wang, L.; Li, Y.; Li, Y.; Sui, Z.; Xu, X. Modulation of pore structure in a microporous carbon for enhanced adsorption of perfluorinated electron specialty gases with efficient separation. *Chem. Eng. J.* **2023**, *477*, No. 147128.

(6) Guo, L.; Fang, X. Mitigation of fully fluorinated greenhouse gas emissions in China and implications for climate change mitigation. *Environ. Sci. Technol.* **2023**, *57*, 19487−19496.

(7) Vileno, E.; LeClair, M. K.; Suib, S. L.; Cutlip, M. B.; Galasso, F. S.; Hardwick, S. J. Thermal decomposition of $NF_3$ with various oxides. *Chem. Mater.* **1996**, *8*, 1217−1221.

(8) Pan, Y.; Gao, Q.; Xu, X. The MgO treated hydrothermally and subsequent MgO@ $Mn_2O_3$ sorbents for $NF_3$ destructive sorption. *Inorg. Chem. Commun.* **2023**, *158*, No. 111570.

(9) Pan, Y.; Li, H.; Zheng, L.; Xu, X. The $Al_2O_3$ and $Mn/Al_2O_3$ sorbents highly utilized in destructive sorption of $NF_3$. *Chin. J. Chem. Eng.* **2024**, *65*, 54−62.

(10) Xu, X.; Gao, Q.; Yin, C.; Pan, Y. $NF_3$ decomposition in the absence of water over some metal oxides coated-$Al_2O_3$ reagents. *J. Environ. Chem. Eng.* **2019**, *7*, No. 103192.

(11) Xu, X.; Sun, L.; Wang, Y. $NF_3$ decomposition over $Al_2O_3$ reagents without water. *J. Nat. Gas Chem.* **2011**, *20*, 418−422.
(12) Furukawa, H.; Cordova, K. E.; O'Keeffe, M.; Yaghi, O. M. The chemistry and applications of metal-organic frameworks. *Science* **2013**, *341*, No. 1230444.
(13) Li, H.; Li, L.; Lin, R.-B.; Zhou, W.; Zhang, Z.; Xiang, S.; Chen, B. Porous metal-organic frameworks for gas storage and separation: Status and challenges. *EnergyChem.* **2019**, *1*, No. 100006.
(14) Wang, S.-M.; Lan, H.-L.; Guan, G.-W.; Yang, Q.-Y. Amino-functionalized microporous MOFs for capturing greenhouse gases $CF_4$ and $NF_3$ with record selectivity. *ACS Appl. Mater. Interfaces* **2022**, *14*, 40072−40081.
(15) Yuan, X.; Cho, M.-K.; Lee, J. G.; Choi, S. W.; Lee, K. B. Upcycling of waste polyethylene terephthalate plastic bottles into porous carbon for $CF_4$ adsorption. *Environ. Pollut.* **2020**, *265*, No. 114868.
(16) Chuah, C. Y.; Lee, Y.; Bae, T.-H. Potential of adsorbents and membranes for SF6 capture and recovery: A review. *Chem. Eng. J.* **2021**, *404*, No. 126577.
(17) Mu, X.; Xue, Y.; Hu, M.; Zhang, P.; Wang, Y.; Li, H.; Li, S.; Zhai, Q. Fine-tuning of pore-space-partitioned metal-organic frameworks for efficient $C_2H_2/C_2H_4$ and $C_2H_2/CO_2$ separation. *Chin. Chem. Lett.* **2023**, *34*, 107296.
(18) Caskey, S. R.; Wong-Foy, A. G.; Matzger, A. J. Dramatic tuning of carbon dioxide uptake via metal substitution in a coordination polymer with cylindrical pores. *J. Am. Chem. Soc.* **2008**, *130*, 10870−10871.
(19) Kim, M.-B.; Lee, S.-J.; Lee, C. Y.; Bae, Y.-S. High $SF_6$ selectivities and capacities in isostructural metal-organic frameworks with proper pore sizes and highly dense unsaturated metal sites. *Micropor. Mesopor. Mater.* **2014**, *190*, 356−361.
(20) Rosi, N. L.; Kim, J.; Eddaoudi, M.; Chen, B.; O'Keeffe, M.; Yaghi, O. M. Rod packings and metal-organic frameworks constructed from rod-shaped secondary building units. *J. Am. Chem. Soc.* **2005**, *127*, 1504−1518.
(21) Dietzel, P. D.; Morita, Y.; Blom, R.; Fjellvåg, H. An in situ high-temperature single-crystal investigation of a dehydrated metal−organic framework compound and field-induced magnetization of one-dimensional metal−oxygen chains. *Angew. Chem. Int. Ed.* **2005**, *117*, 6512−6516.
(22) Dietzel, P. D.; Panella, B.; Hirscher, M.; Blom, R.; Fjellvåg, H. Hydrogen adsorption in a nickel based coordination polymer with open metal sites in the cylindrical cavities of the desolvated framework. *Chem. Commun.* **2006**, 959−961.
(23) Dietzel, P. D.; Blom, R.; Fjellvåg, H. Base-induced formation of two magnesium metal-organic framework compounds with a bifunctional tetratopic ligand. *Eur. J. Inorg. Chem.* **2008**, *2008* (23), 3624−3632.
(24) Bae, Y. S.; Lee, C. Y.; Kim, K. C.; Farha, O. K.; Nickias, P.; Hupp, J. T.; Nguyen, S. T.; Snurr, R. Q. High propene/propane selectivity in isostructural metal−organic frameworks with high densities of open metal sites. *Angew. Chem. Int. Ed.* **2012**, *124*, 1893−1896.
(25) Dietzel, P. D.; Johnsen, R. E.; Fjellvåg, H.; Bordiga, S.; Groppo, E.; Chavan, S.; Blom, R. Adsorption properties and structure of $CO_2$ adsorbed on open coordination sites of metal−organic framework $Ni_2$(dhtp) from gas adsorption, IR spectroscopy and X-ray diffraction. *Chem. Commun.* **2008**, 5125−5127.
(26) Diaz-Garcia, M.; Mayoral, A.; Diaz, I.; Sanchez-Sanchez, M. Nanoscaled M-MOF-74 materials prepared at room temperature. *Cryst. Growth Des.* **2014**, *14*, 2479−2487.
(27) Zhang, W.; Wu, Y.; Li, Y.; Chen, S.; Fu, Y.; Zhang, Z.; Yan, T.; Wang, S.; Ma, H. Fluorine-functionalized porous organic polymers for durable F-gas capture from semiconductor etching exhaust. *Macromolecules* **2022**, *55*, 1435−1444.
(28) Wu, Y.; Yan, T.; Zhang, W. X.; Chen, S. H.; Fu, Y.; Zhang, Z. S.; Ma, H. P. Adsorption interface-induced H···F charge transfer in ultramicroporous metal−organic frameworks for perfluorinated gas separation. *Ind. Eng. Chem. Res.* **2022**, *61*, 13603−13611.
(29) Wu, Y.; Wang, S. S.; Zhang, W. X.; Chen, S. H.; Zhang, Z. H.; Yang, B. L.; Li, S. P.; Ma, H. P. Enhancing perfluorinated electron specialty gases separation selectivity in ultra-microporous metal organic framework. *Sep. Purif. Technol.* **2022**, *289*, No. 120739.
(30) Fu, W.; Wang, J.; Li, Y.; Sui, Z.; Xiao, B.; Xu, X. Highly-efficient separation of $SF_6/N_2$ and $NF_3/N_2$ with record selectivity on one-step synthesized carbon nanosheet. *Sep. Purif. Technol.* **2024**, *330*, No. 125496.


https://doi.org/10.1021/cbe.3c00096
*Chem Bio Eng.* 2024, 1, 535−540